

Synthetic Augmentation with Large-scale Unconditional Pre-training

Jiarong Ye^{1*}, Haomiao Ni^{1*}, Peng Jin¹, Sharon X. Huang¹, and Yuan Xue^{2,3}

¹ The Pennsylvania State University, University Park, Pennsylvania, USA

² Johns Hopkins University, Baltimore, Maryland, USA

³ The Ohio State University, Columbus, Ohio, USA

Yuan.Xue@osumc.edu

Abstract. Deep learning based medical image recognition systems often require a substantial amount of training data with expert annotations, which can be expensive and time-consuming to obtain. Recently, synthetic augmentation techniques have been proposed to mitigate the issue by generating realistic images conditioned on class labels. However, the effectiveness of these methods heavily depends on the representation capability of the trained generative model, which cannot be guaranteed without sufficient labeled training data. To further reduce the dependency on annotated data, we propose a synthetic augmentation method called HistoDiffusion, which can be pre-trained on large-scale unlabeled datasets and later applied to a small-scale labeled dataset for augmented training. In particular, we train a latent diffusion model (LDM) on diverse unlabeled datasets to learn common features and generate realistic images without conditional inputs. Then, we fine-tune the model with classifier guidance in latent space on an unseen labeled dataset so that the model can synthesize images of specific categories. Additionally, we adopt a selective mechanism to only add synthetic samples with high confidence of matching to target labels. We evaluate our proposed method by pre-training on three histopathology datasets and testing on a histopathology dataset of colorectal cancer (CRC) excluded from the pre-training datasets. With HistoDiffusion augmentation, the classification accuracy of a backbone classifier is remarkably improved by 6.4% using a small set of the original labels. Our code is available at <https://github.com/karenyyy/HistoDiffAug>.

1 Introduction

The recent advancements in medical image recognition systems have greatly benefited from deep learning techniques [15, 28]. Large-scale well-annotated datasets are one of the key components for training deep learning models to achieve satisfactory results [3, 17]. However, unlike natural images in computer vision, the number of medical images with expert annotations is often limited by the high labeling cost and privacy concerns. To overcome this challenge, a natural choice

* These authors contributed equally to this work.

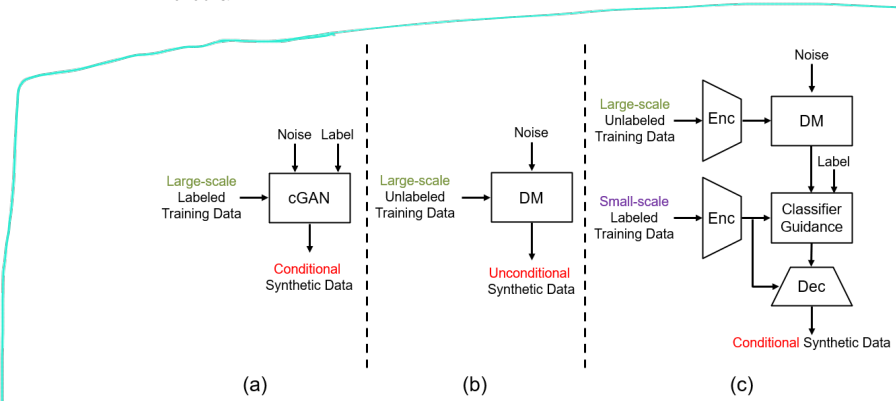


Fig. 1. Comparison between different deep generative models for synthetic augmentation. (a) cGAN-based method which requires relatively large-scale annotated training data; (b) Diffusion model (DM) which cannot take conditional input; (c) Our proposed HistoDiffusion model that can be pretrained on large-scale unannotated data and later applied to *unseen* small-scale annotated data for augmentation.

is to employ data augmentation to increase the number of training samples. Although conventional augmentation techniques [23] such as flipping and cropping can be directly applied to medical images, they merely improve the diversity of datasets, thus leading to marginal performance gains [1]. Another group of studies employ conditional generative adversarial networks (cGANs) [10] to synthesize visually appealing medical images that closely resemble those in the original datasets [36,37]. While existing works have proven effective in improving the performance of downstream models to some extent, a sufficient amount of labeled data is still required to adequately train models to generate decent-quality images. More recently, diffusion models have become popular for natural image generation due to their impressive results and training stability [4,13,31]. A few studies have also demonstrated the potential of diffusion models for medical image synthesis [19,24].

Although annotated data is typically hard to acquire for medical images, unannotated data is often more accessible. To mitigate the issue existed in current cGAN-based synthetic augmentation methods [8,36,37,38], in this work, we propose to leverage the diffusion model with unlabeled pre-training to reduce the dependency on the amount of labeled data (see comparisons in Fig. 1). We propose a novel synthetic augmentation method, named HistoDiffusion, which can be pre-trained on large-scale unannotated datasets and adapted to small-scale annotated datasets for augmented training. Specifically, we first employ a latent diffusion model (LDM) and train it on a collection of unlabeled datasets from multiple sources. This large-scale pre-training enables the model to learn common yet diverse image characteristics and generate realistic medical images. Second, given a small labeled dataset that does not exist in the pre-training datasets, the decoder of the LDM is fine-tuned using annotations to adapt to the domain shift. Synthetic images are then generated with classifier guidance [4] in the latent space. Following the prior work [36], we select generated images based

on the confidence of target labels and feature similarity to real labeled images. We evaluate our proposed method on a histopathology image dataset of colorectal cancer (CRC). Experiment results show that when presented with limited annotations, the classifier trained with our augmentation method outperforms the ones trained with the prior cGAN-based methods. Our experimental results show that once HistoDiffusion is well pre-trained using large datasets, it can be applied to any future incoming small dataset with minimal fine-tuning and may substantially improve the flexibility and efficacy of synthetic augmentation.

2 Methodology

Fig. 2 illustrates the overall architecture of our proposed method. First, we train an LDM on a large-scale set of unlabeled datasets collected from multiple sources. We then fine-tune the decoder of this pretrained LDM on a small labeled dataset. To enable conditional image synthesis, we also train a latent classifier on the same labeled dataset to guide the diffusion model in LDM. Once the classifier is trained, we apply the fine-tuned LDM to generate a pool of candidate images conditioned on the target class labels. These candidate images are then passed through the image selection module to filter out any low-quality results. Finally, we can train downstream classification models on the expanded training data, which includes the selected images, and then use them to perform inference on test data. In this section, we will first introduce the background of diffusion models and then present details about the HistoDiffusion model.

2.1 Diffusion Models

Diffusion models (DM) [13,30,32] are probabilistic models that are designed to learn a data distribution. Given a sample from the data distribution $z_0 \sim q(z_0)$, the DM *forward* process produces a Markov chain z_1, \dots, z_T by gradually adding Gaussian noise to z_0 based on a variance schedule β_1, \dots, β_T , that is:

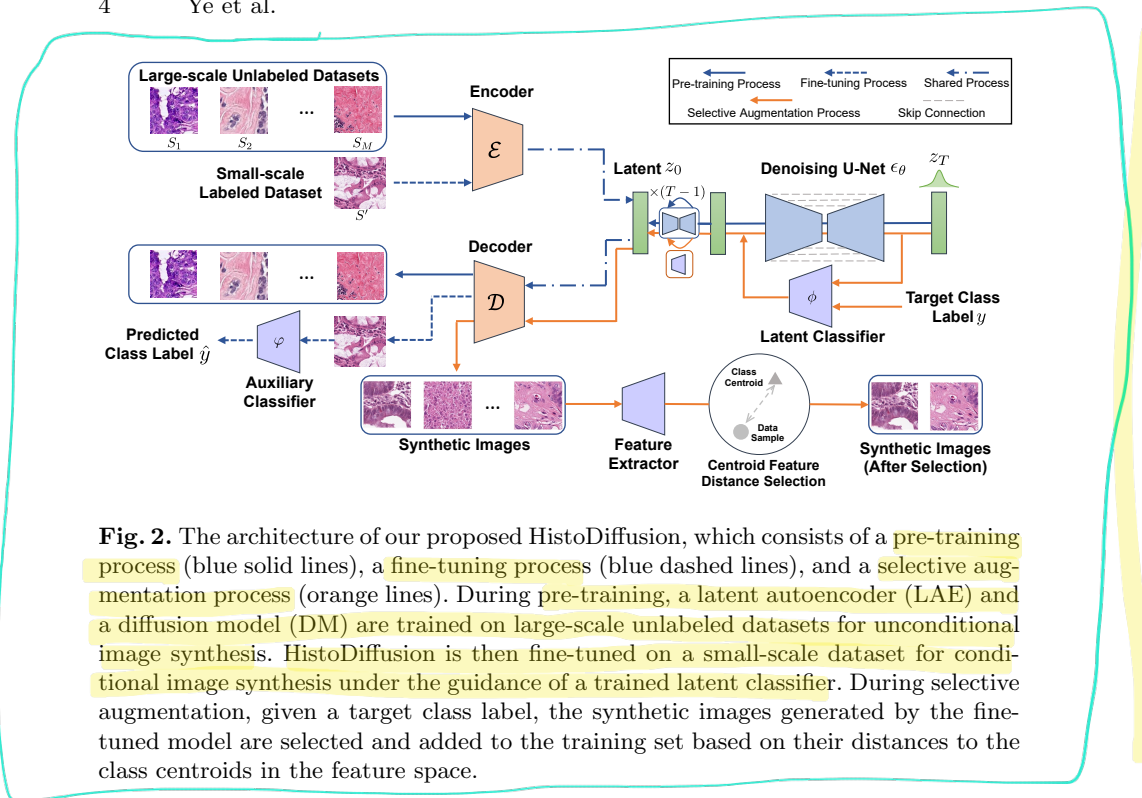
$$q(z_t | z_{t-1}) = \mathcal{N}(z_t; \sqrt{1 - \beta_t} z_{t-1}, \beta_t \mathbf{I}), \quad (1)$$

where variances β_t are constants. If β_t are small, the posterior $q(z_{t-1} | z_t)$ can be well approximated by diagonal Gaussian [21,30]. Furthermore, when the T of the chain is large enough, z_T can be well approximated by standard Gaussian distribution $\mathcal{N}(\mathbf{0}, \mathbf{I})$. These suggest that the true posterior $q(z_{t-1} | z_t)$ can be estimated by $p_\theta(z_{t-1} | z_t)$ defined as [22]:

$$p_\theta(z_{t-1} | z_t) = \mathcal{N}(z_{t-1}; \mu_\theta(z_t), \Sigma_\theta(z_t)). \quad (2)$$

The DM *reverse* process (also known as *sampling*) then generates samples $z_0 \sim p_\theta(z_0)$ by initiating a Markov chain with Gaussian noise $z_T \sim \mathcal{N}(\mathbf{0}, \mathbf{I})$ and progressively decreasing noise in the chain of $z_{T-1}, z_{T-2}, \dots, z_0$ using the learnt $p_\theta(z_{t-1} | z_t)$. To learn $p_\theta(z_{t-1} | z_t)$, Gaussian noise ϵ is added to z_0 to generate samples $z_t \sim q(z_t | z_0)$, then a model ϵ_θ is trained to predict ϵ using the following mean-squared error loss:

$$L_{\text{DM}} = \mathbb{E}_{t \sim \mathcal{U}(1, T), z_0 \sim q(z_0), \epsilon \sim \mathcal{N}(\mathbf{0}, \mathbf{I})} [\|\epsilon - \epsilon_\theta(z_t, t)\|^2], \quad (3)$$



where time step t is uniformly sampled from $\{1, \dots, T\}$. Then $\mu_\theta(z_t)$ and $\Sigma_\theta(z_t)$ in Eq. 2 can be derived from $\epsilon_\theta(z_t, t)$ to model $p_\theta(z_{t-1}|z_t)$ [13, 22]. The denoising model ϵ_θ is typically implemented using a time-conditioned U-Net [27] with residual blocks [11] and self-attention layers [35]. Sinusoidal position embedding [35] is also usually used to specify the time step t to ϵ_θ .

2.2 HistoDiffusion

Model Architecture. Our proposed HistoDiffusion is built on Latent Diffusion Models (LDM) [26], which requires fewer computational resources without degradation in performance, compared to prior works [4, 15, 28]. LDM first trains a latent autoencoder (LAE) [16] to encode images as lower-dimensional latent representations and then learns a diffusion model (DM) for image synthesis by modeling the latent space of the trained LAE. Particularly, the encoder \mathcal{E} of the LAE encodes the input image $x \in \mathbb{R}^{H \times W \times 3}$ into a latent representation $z = \mathcal{E}(x) \in \mathbb{R}^{h \times w \times c}$ in a lower-dimensional latent space \mathcal{Z} . Here H and W are the height and width of image x , and h , w , and c are the height, width, and channel of latent z , respectively. The latent z is then passed into the decoder \mathcal{D} to reconstruct the image $\hat{x} = \mathcal{D}(z)$. Through this process, the compositional features from the image space \mathcal{X} can be extracted to form the latent space \mathcal{Z} , and we then model the distribution of \mathcal{Z} by learning a DM. For the DM in

LDM, both the forward and reverse sampling processes are performed in the latent space \mathcal{Z} instead of the original image space \mathcal{X} .

Unconditional Large-scale Pre-training. To ensure the latent space \mathcal{Z} can cover features of various data types, we first pre-train our proposed HistoDiffusion on large-scale unlabeled datasets. Specifically, we gather unlabeled images from M different sources to construct a large-scale set of datasets $\mathcal{S} = \{S_1, S_2, \dots, S_M\}$. We then train an LAE using the data from \mathcal{S} with the following self-reconstruction loss to learn a powerful latent space \mathcal{Z} that can describe diverse features:

$$L_{\text{LAE}} = \mathcal{L}_{\text{rec}}(\hat{x}, x) + \lambda_{\text{KL}} D_{\text{KL}}(q(z)||\mathcal{N}(\mathbf{0}, \mathbf{I})) , \quad (4)$$

where \mathcal{L}_{rec} is the loss measuring the difference between the output reconstructed image \hat{x} and the input ground truth image x . Here we implement \mathcal{L}_{rec} with a combination of a pixel-wise L_1 loss, a perceptual loss [39], and a patch-base adversarial loss [6,7]. To avoid arbitrarily high-variance latent spaces, we also add a KL regularization term D_{KL} [16,26] to constrain the variance of the latent space \mathcal{Z} with a slight KL-penalty.

After training the LAE, we fixed the trained encoder \mathcal{E} and then train a DM with the loss L_{DM} in Eq. 3 to model \mathcal{E} 's latent space \mathcal{Z} . Here $z_0 = \mathcal{E}(x)$ in Eq. 3. Once the DM is trained, we can use denoising model ϵ_θ in the DM reverse sampling process to synthesize a novel latent $\tilde{z}_0 \in \mathbb{R}^{h \times w \times c}$ and employ the trained decoder \mathcal{D} to generate a new image $\tilde{x} = \mathcal{D}(\tilde{z}_0)$, which should satisfy the similar distribution as the data in \mathcal{S} .

Conditional Small-scale Fine-tuning. Using the LAE and DM pretrained on \mathcal{S} , we can only generate the new image \tilde{x} following the similar distribution in \mathcal{S} . To generalize our HistoDiffusion to the small-scale labeled dataset S' collected from a different source (*i.e.*, $S' \not\subset \mathcal{S}$), we further fine-tune HistoDiffusion using the labeled data from S' . Let y be the label of image x in S' . To minimize the training cost, we fix both the trained encoder \mathcal{E} and trained DM model ϵ_θ to keep latent space \mathcal{Z} unchanged. Then we only fine-tune the decoder \mathcal{D} using labeled data (x, y) from S' with the following loss function:

$$L_{\mathcal{D}} = \mathcal{L}_{\text{rec}}(\hat{x}, x) + \lambda_{\text{CE}} \mathcal{L}_{\text{CE}}(\varphi(\hat{x}), y) , \quad (5)$$

where $\mathcal{L}_{\text{rec}}(\hat{x}, x)$ is the self-reconstruction loss between the output reconstructed image $\hat{x} = \mathcal{D}(\mathcal{E}(x))$ and the input ground truth image x . To enhance the correlation between the decoder output \hat{x} and label y , we also add an auxiliary image classifier φ trained with (x, y) on the top of \mathcal{D} and impose the cross-entropy classification loss \mathcal{L}_{CE} when fine-tuning \mathcal{D} . λ_{CE} is the balancing parameter. We annotate this fine-tuned decoder as \mathcal{D}' for differentiation.

Classifier-guided Conditional Synthesis. To enable conditional image generation with our HistoDiffusion, we further apply the classifier-guided diffusion sampling proposed in [4,29,30,33] using the labeled data (x, y) from small-scale labeled dataset S' . We first utilize the trained encoder \mathcal{E} to encode the data x from S' as latent z_0 . Then we train a time-dependent latent classifier ϕ with paired (z_t, y) using the following loss function:

$$L_\phi = \mathcal{L}_{\text{CE}}(\phi(z_t), y) , \quad (6)$$

where $z_t \sim q(z_t|z_0)$ is the noisy version of z_0 at the time step t during the DM forward process, and \mathcal{L}_{CE} is the cross-entropy classification loss. Based on the trained unconditional diffusion model ϵ_θ , and a classifier ϕ trained on noisy input z_t , we enable conditional diffusion sampling by perturbing the reverse-process mean with the gradient of the log probability $p_\phi(y|z_t)$ of a target class y predicted by the classifier ϕ as follows:

$$\hat{\mu}_\theta(z_t|y) = \mu_\theta(z_t) + g \cdot \nabla_{z_t} \log p_\phi(y|z_t) , \quad (7)$$

where g is the guidance scale. Then the DM reverse process in HistoDiffusion can finally generate a novel latent \tilde{z}_0 satisfying the class condition y through a Markov chain starting with a standard Gaussian noise $z_T \sim \mathcal{N}(\mathbf{0}, \mathbf{I})$ using $p_{\theta,\phi}(z_{t-1}|z_t, y)$ defined as follows:

$$p_{\theta,\phi}(z_{t-1}|z_t, y) = \mathcal{N}(z_{t-1}; \hat{\mu}_\theta(z_t|y), \Sigma_\theta(z_t)) . \quad (8)$$

The final image \tilde{x} of class y can be generated by applying the fine-tuned decoder \mathcal{D}' , i.e., $\tilde{x} = \mathcal{D}'(\tilde{z}_0)$.

Selective Augmentation. To further improve the efficacy of synthetic augmentation, we follow [36] to selectively add synthetic images to the original labeled training data based on centroid feature distance. The augmentation ratio is defined as the ratio between the selected synthetic images and the original training images. More results are demonstrated later in Table 1.

3 Experiments

Datasets. We employ three public datasets of histopathology images during the large-scale pre-training procedure. The first one is the H&E breast cancer dataset [2], containing 312,320 patches extracted from the hematoxylin & eosin (H&E) stained human breast cancer tissue micro-array (TMA) images [18]. Each patch has a resolution of 224×224 . The second dataset is PanNuke [9], a pan-cancer histology dataset for nuclei instance segmentation and classification. The PanNuke dataset includes 7,901 patches of 19 types of H&E stained tissues obtained from multiple data sources, and each patch has a unified size of 256×256 pixels. The third dataset is TCGA-BRCA-A2/E2 [34], a subset derived from the TCGA-BRCA breast cancer histology dataset [20]. The subset consists of 482,958 patches with a resolution of 256×256 . Overall, there are 803,179 patches used for pre-training. As for fine-tuning and evaluation, we employ the NCT-CRC-HE-100K dataset that contains 100,000 patches from H&E stained histological images of human colorectal cancer (CRC) and normal tissue. The patches have been divided into 9 classes: Adipose (ADI), background (BACK), debris (DEB), lymphocytes (LYM), mucus (MUC), smooth muscle (MUS), normal colon mucosa (NORM), cancer-associated stroma (STR), colorectal adenocarcinoma epithelium (TUM). The resolution of each patch is 224×224 .

To replicate a scenario where only a small annotated dataset is available for training, we have opted to utilize a subset of 5,000 (5%) samples for fine-tuning. This subset has been carefully selected through an even sampling without replacement from each tissue type present in the train set. It is worth noting that

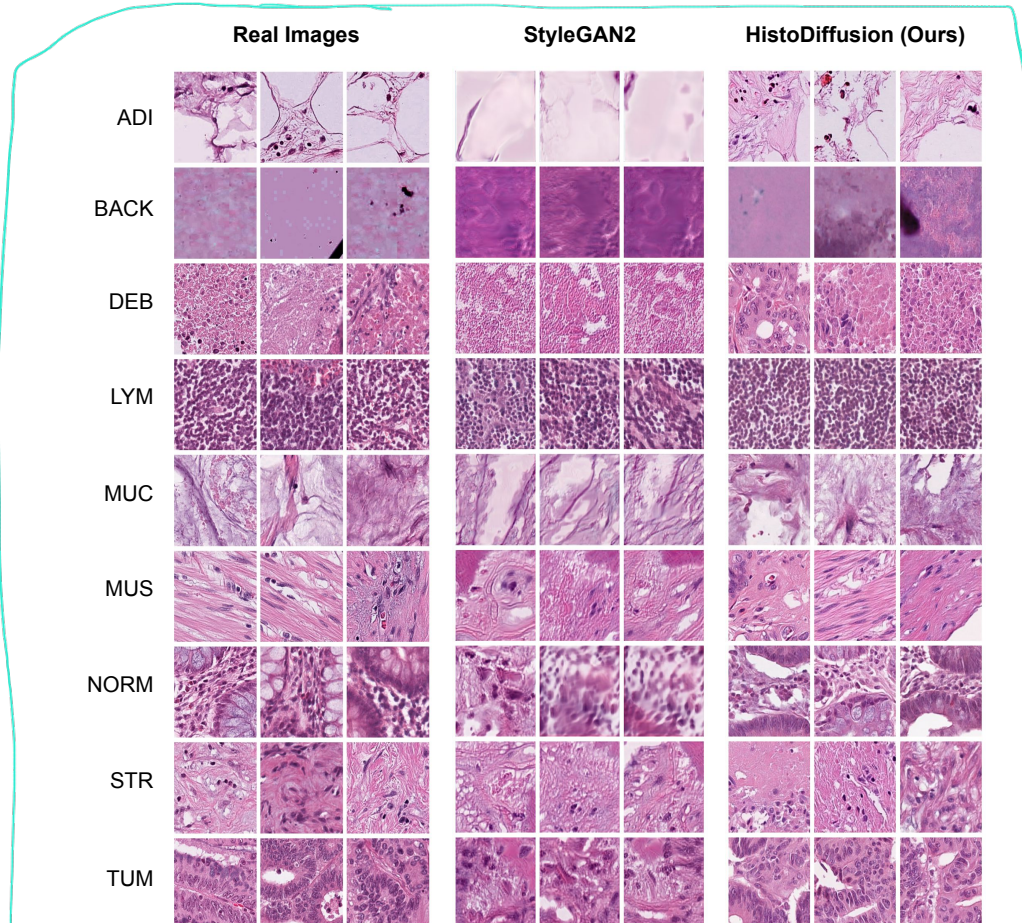


Fig. 3. Comparison of real images from training subset, synthesized images generated by StyleGAN2 [14] and our proposed HistoDiffusion (zoom in for clear observation). Qualitatively, our synthesized results contain more realistic and diagnosable patterns than results synthesized from StyleGAN2.

the labels for these samples have been kept, which allows the fine-tuning process to be guided by labeled data, leading to better predictions on the specific task or domain being trained. By ensuring that the fine-tuning process is representative of the entire dataset through even sampling from each tissue type, we can eliminate bias towards any particular tissue type. We evaluate the fine-tuned model on the official test set. The related data use declaration and acknowledgment can be found in our supplementary materials.

Evaluation Metrics. We employ Fréchet Inception Distance (FID) score [12] to assess the image quality of the synthetic samples. We further compute the accuracy, F1-score, sensitivity, and specificity of the downstream classifiers to evaluate the performance gain from different augmentation methods.

Table 1. Quantitative comparison results of synthetic image quality and augmented classification. “Random” refers to directly augmenting the training dataset with synthesized images without any image selections while “selective” indicates applying selective module [36] to filter out low-quality images. The number ($X\%$) suggests that the number of the synthesized images is $X\%$ of the original training set.

	FID↓	Accuracy↑	F1 Score↑	Sensitivity↑	Specificity↑
Baseline (5% real images)	/	0.855	0.850	0.855	0.983
StyleGAN2 [14]					
+ random 50%	5.714	0.860	0.856	0.860	0.980
+ selective [36] 50%	5.088	0.868	0.861	0.867	0.978
100%	5.927	0.879	0.876	0.879	0.982
200%	7.550	0.895	0.888	0.895	0.983
300%	10.643	0.898	0.896	0.898	0.987
HistoDiffusion (Ours)					
+ random 50%	4.921	0.870	0.869	0.870	0.982
+ selective [36] 50%	4.544	0.891	0.888	0.891	0.983
100%	3.874	0.903	0.902	0.903	0.991
200%	4.583	0.919	0.916	0.919	0.992
300%	8.326	0.910	0.912	0.910	0.988

Model Implementation. All the patches are resized to $256 \times 256 \times 3$ before being passed into the models. Our implementation of HistoDiffusion basically follows the LDM-4 [26] architecture, where the input is downsampled by a factor of 4, resulting in a latent representation with dimensions of $64 \times 64 \times 3$. We use 1000 timesteps ($T = 1000$) for the training of diffusion model and sample with classifier-free guidance scale $g = 1.0$ and 200 DDIM steps. The latent classifier ϕ is constructed using the encoder architecture of the LAE and an additional attention pooling layer [25] added before the output layer.

We use the same architecture for the auxiliary image classifier φ . For downstream evaluation, we implement the classifier using the ViT-B/16 architecture [5] in all experiments to ensure fair comparisons. The default hyper-parameter settings provided in their officially released codebases are followed.

Comparsion to state-of-the-art. We compare our proposed HistoDiffusion with the current state-of-the-art cGAN-based method [36]. We employ StyleGAN2 [14] as the backbone generative model for cGAN-based synthesis. To ensure a fair comparison, all images synthesized by StyleGAN2 and HistoDiffusion model are further selected based on feature centroid distances [36]. More implementation details of our proposed HistoDiffusion, StyleGAN2, and baseline classifier can also be found in our supplementary materials.

Result Analysis. As shown in Table 1, under the same synthetic augmentation setting, HistoDiffusion shows better FID scores and outperforms the state-of-the-art cGAN model StyleGAN2 in all classification metrics. A qualitative comparison between synthetic images by HistoDiffusion and StyleGAN2 can be found in Fig. 3, where HistoDiffusion consistently generates more realistic im-

ages matching the given class conditions than StyleGAN2, especially for classes ADI and BACK.

When augmenting the training dataset with different numbers of images synthesized from HistoDiffusion and StyleGAN2, one can observe that when increasing the ratio of synthesized data to 100%, the FID score of StyleGAN2 increases quickly and can become even worse than the one without using image selection strategy. In contrast, HistoDiffusion can keep synthesizing high-quality images until the augmentation ratio reaches 300%. Regarding classification performance improvement of the baseline classifier, the accuracy and F1 score of using HistoDiffusion augmentation are increased by up to **6.4%** and **6.6%**, respectively. Even when not using the image selection module to filter out the low-quality results (*i.e.*, +random 50%), our HistoDiffusion can still improve the accuracy by 1.5%. The robustness and effectiveness of HistoDiffusion can be attributed to the unconditional large-scale pre-training, our specially-designed conditional fine-tuning, and classifier-guided generation, among others.

4 Conclusions

In this study, we have introduced a novel synthetic augmentation technique, termed HistoDiffusion, to enhance the performance of medical image recognition systems. HistoDiffusion leverages multiple unlabeled datasets for large-scale, unconditional pre-training, while employing a labeled dataset for small-scale conditional fine-tuning. Experiment results on a histopathology image dataset excluded from the pre-training demonstrate that given limited labels, HistoDiffusion with image selection remarkably enhances the classification performance of the baseline model, and can potentially handle any future incoming small dataset for augmented training using the same pre-trained model.

References

- Chen, Y., Yang, X.H., Wei, Z., Heidari, A.A., Zheng, N., Li, Z., Chen, H., Hu, H., Zhou, Q., Guan, Q.: Generative adversarial networks in medical image augmentation: a review. *Comput. Biol. Med.* p. 105382 (2022)
- Claudio Quiros, A., Murray-Smith, R., Yuan, K.: Pathologygan: Learning deep representations of cancer tissue. *MELBA* **2021**(4), 1–48 (2021)
- Deng, J., Dong, W., Socher, R., Li, L.J., Li, K., Fei-Fei, L.: Imagenet: A large-scale hierarchical image database. In: *CVPR*. pp. 248–255. Ieee (2009)
- Dhariwal, P., Nichol, A.: Diffusion models beat gans on image synthesis. *NeurIPS* **34**, 8780–8794 (2021)
- Dosovitskiy, A., Beyer, L., Kolesnikov, A., Weissenborn, D., Zhai, X., Unterthiner, T., Dehghani, M., Minderer, M., Heigold, G., Gelly, S., et al.: An image is worth 16x16 words: Transformers for image recognition at scale. *ICLR* (2021)
- Dosovitskiy, A., Brox, T.: Generating images with perceptual similarity metrics based on deep networks. *NeurIPS* **29** (2016)
- Esser, P., Rombach, R., Ommer, B.: Taming transformers for high-resolution image synthesis. In: *CVPR*. pp. 12873–12883 (2021)

8. Frid-Adar, M., Diamant, I., Klang, E., Amitai, M., Goldberger, J., Greenspan, H.: Gan-based synthetic medical image augmentation for increased cnn performance in liver lesion classification. *Neurocomputing* **321**, 321–331 (2018)
9. Gamper, J., Alemi Koohbanani, N., Benet, K., Khuram, A., Rajpoot, N.: Pan-nuke: an open pan-cancer histology dataset for nuclei instance segmentation and classification. In: ECDP. pp. 11–19. Springer (2019)
10. Goodfellow, I., Pouget-Abadie, J., Mirza, M., Xu, B., Warde-Farley, D., Ozair, S., Courville, A., Bengio, Y.: Generative adversarial networks. *Communications of the ACM* **63**(11), 139–144 (2020)
11. He, K., Zhang, X., Ren, S., Sun, J.: Deep residual learning for image recognition. In: CVPR. pp. 770–778 (2016)
12. Heusel, M., Ramsauer, H., Unterthiner, T., Nessler, B., Hochreiter, S.: Gans trained by a two time-scale update rule converge to a local nash equilibrium. *NeurIPS* **30** (2017)
13. Ho, J., Jain, A., Abbeel, P.: Denoising diffusion probabilistic models. *NeurIPS* **33**, 6840–6851 (2020)
14. Karras, T., Laine, S., Aittala, M., Hellsten, J., Lehtinen, J., Aila, T.: Analyzing and improving the image quality of stylegan. In: CVPR. pp. 8110–8119 (2020)
15. Ker, J., Wang, L., Rao, J., Lim, T.: Deep learning applications in medical image analysis. *Ieee Access* **6**, 9375–9389 (2017)
16. Kingma, D.P., Welling, M.: Auto-encoding variational bayes. arXiv (2013)
17. Lin, T.Y., Maire, M., Belongie, S., Hays, J., Perona, P., Ramanan, D., Dollár, P., Zitnick, C.L.: Microsoft coco: Common objects in context. In: ECCV. pp. 740–755. Springer (2014)
18. Marinelli, R.J., Montgomery, K., Liu, C.L., Shah, N.H., Prapong, W., Nitzberg, M., Zachariah, Z.K., Sherlock, G.J., Natkunam, Y., West, R.B., et al.: The stanford tissue microarray database. *Nucleic acids research* **36**(suppl_1), D871–D877 (2007)
19. Moghadam, P.A., Van Dalen, S., Martin, K.C., Lennerz, J., Yip, S., Farahani, H., Bashashati, A.: A morphology focused diffusion probabilistic model for synthesis of histopathology images. In: WACV. pp. 2000–2009 (2023)
20. Network, T.C.G.A.: Comprehensive molecular portraits of human breast tumours. *Nature* **490**(7418), 61–70 (2012)
21. Nichol, A., Dhariwal, P., Ramesh, A., Shyam, P., Mishkin, P., McGrew, B., Sutskever, I., Chen, M.: Glide: Towards photorealistic image generation and editing with text-guided diffusion models. arXiv (2021)
22. Nichol, A.Q., Dhariwal, P.: Improved denoising diffusion probabilistic models. In: ICML. pp. 8162–8171. PMLR (2021)
23. Perez, L., Wang, J.: The effectiveness of data augmentation in image classification using deep learning. arXiv (2017)
24. Pinaya, W.H., Tudosi, P.D., Dafflon, J., Da Costa, P.F., Fernandez, V., Nachev, P., Ourselin, S., Cardoso, M.J.: Brain imaging generation with latent diffusion models. In: DGM4MICCAI. pp. 117–126. Springer (2022)
25. Radford, A., Kim, J.W., Hallacy, C., Ramesh, A., Goh, G., Agarwal, S., Sastry, G., Askell, A., Mishkin, P., Clark, J., et al.: Learning transferable visual models from natural language supervision. In: ICML. pp. 8748–8763. PMLR (2021)
26. Rombach, R., Blattmann, A., Lorenz, D., Esser, P., Ommer, B.: High-resolution image synthesis with latent diffusion models. In: CVPR. pp. 10684–10695 (2022)
27. Ronneberger, O., Fischer, P., Brox, T.: U-net: Convolutional networks for biomedical image segmentation. In: MICCAI. pp. 234–241. Springer (2015)
28. Shen, D., Wu, G., Suk, H.I.: Deep learning in medical image analysis. *Annu. Rev. Biomed. Eng.* **19**, 221–248 (2017)

29. Shi, C., Ni, H., Li, K., Han, S., Liang, M., Min, M.R.: Exploring compositional visual generation with latent classifier guidance. In: CVPR. pp. 853–862 (2023)
30. Sohl-Dickstein, J., Weiss, E., Maheswaranathan, N., Ganguli, S.: Deep unsupervised learning using nonequilibrium thermodynamics. In: ICML. pp. 2256–2265 (2015)
31. Song, J., Meng, C., Ermon, S.: Denoising diffusion implicit models. arXiv (2020)
32. Song, Y., Ermon, S.: Generative modeling by estimating gradients of the data distribution. NeurIPS **32** (2019)
33. Song, Y., Sohl-Dickstein, J., Kingma, D.P., Kumar, A., Ermon, S., Poole, B.: Score-based generative modeling through stochastic differential equations. arXiv (2020)
34. van Treeck, M., Cifci, D., Laleh, N.G., Saldanha, O.L., Loeffler, C.M., Hewitt, K.J., Muti, H.S., Echle, A., Seibel, T., Seraphin, T.P., et al.: Deepmed: A unified, modular pipeline for end-to-end deep learning in computational pathology. BioRxiv pp. 2021–12 (2021)
35. Vaswani, A., Shazeer, N., Parmar, N., Uszkoreit, J., Jones, L., Gomez, A.N., Kaiser, L., Polosukhin, I.: Attention is all you need. NeurIPS **30** (2017)
36. Xue, Y., Ye, J., Zhou, Q., Long, L.R., Antani, S., Xue, Z., Cornwell, C., Zaino, R., Cheng, K.C., Huang, X.: Selective synthetic augmentation with histogan for improved histopathology image classification. Med. Image Anal. **67**, 101816 (2021)
37. Xue, Y., Zhou, Q., Ye, J., Long, L.R., Antani, S., Cornwell, C., Xue, Z., Huang, X.: Synthetic augmentation and feature-based filtering for improved cervical histopathology image classification. In: MICCAI. pp. 387–396. Springer (2019)
38. Ye, J., Xue, Y., Long, L.R., Antani, S., Xue, Z., Cheng, K.C., Huang, X.: Synthetic sample selection via reinforcement learning. In: MICCAI. pp. 53–63. Springer (2020)
39. Zhang, R., Isola, P., Efros, A.A., Shechtman, E., Wang, O.: The unreasonable effectiveness of deep features as a perceptual metric. In: CVPR. pp. 586–595 (2018)

Supplementary Materials

Table 1. Quantitative ablation study results of synthetic image quality and augmented classification performance from HistoDiffusion without conditional small-scale fine-tuning and HistoDiffusion trained with only a small-scaled dataset (5% real images). Compared with the final HistoDiffusion, the model without conditional fine-tuning generates images that drastically differ from real images, resulting in high FID scores, whilst the model trained without any pre-training leads to worse classification performance. For the best model trained using 200% synthetic images, the accuracy and F1 score are still **2.4%** and **2.2%** lower than the final model, respectively.

	FID↓	Accuracy↑	F1 Score↑	Sensitivity↑	Specificity↑
HistoDiffusion (w/o conditional small-scale fine-tuning)					
+ random 50%	18.254	0.865	0.867	0.865	0.986
+ selective 50%	19.887	0.875	0.870	0.875	0.982
100%	18.418	0.880	0.879	0.880	0.985
200%	19.229	0.897	0.892	0.897	0.989
300%	21.682	0.905	0.908	0.905	0.988
HistoDiffusion (w/o unconditional large-scale pre-training)					
+ random 50%	5.687	0.870	0.867	0.870	0.984
+ selective 50%	5.256	0.884	0.882	0.884	0.986
100%	4.387	0.890	0.891	0.890	0.988
200%	3.618	0.895	0.894	0.895	0.988
300%	4.446	0.892	0.887	0.892	0.983

Table 2. Implementation details of each modules in HistoDiffusion, baseline classifier, and the baseline StyleGAN2. All models are trained on NVIDIA Quadro RTX 6000 GPUs with 24GB RAM.

	Latent Autoencoder	Diffusion Models	Latent Classifier	Auxiliary Classifier	Fine-tuned Decoder	Baseline Classifier	StyleGAN2
Batch size	6	4	32	64	4	128	64
Training epochs	10	10	100	100	50	200	100
Learning rate	4.5e-6	5.0e-5	5.0e-5	5.0e-5	5.0e-5	1.0e-4	2.0e-4
Optimizer	Adam	AdamW	AdamW	Adam	Adam	AdamW	Adam
Loss weights λ	1.0e-6 (λ_{KL})	-	-	-	1.0 (λ_{CE})	-	-
Guidance scale g	-	-	1.0	-	-	-	-
Noise schedule	-	Linear	-	-	-	-	-

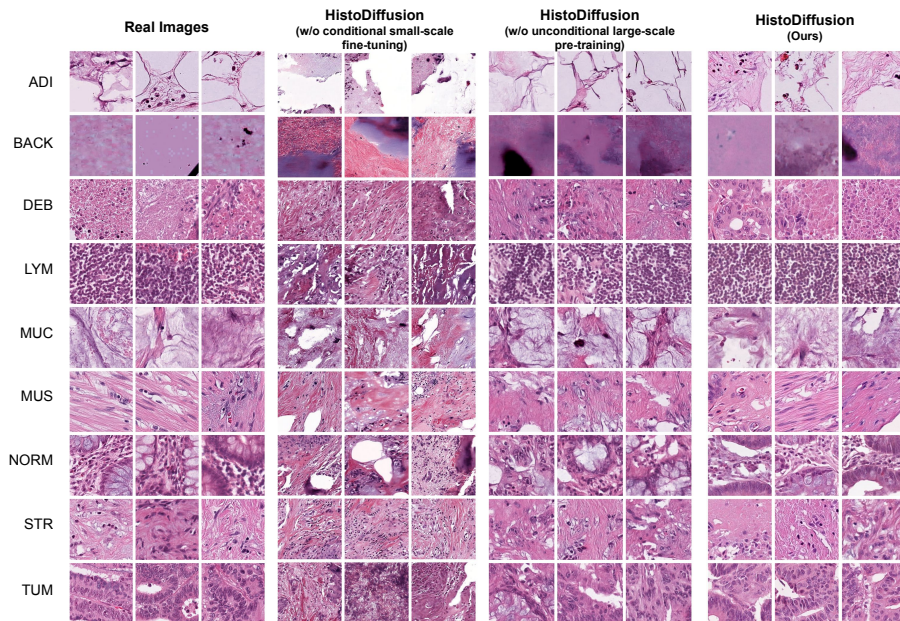


Fig. 1. Qualitative visualization of synthetic images generated by our proposed HistoDiffusion, HistoDiffusion without conditional small-scale fine-tuning, and HistoDiffusion trained using only a small-scaled dataset of 5% real images (*i.e.*, without using unconditional large-scale pre-training). Compared with our final HistoDiffusion, [HistoDiffusion without conditional fine-tuning] sometimes fails to generate images that contain correct corresponding characteristics implied by the class condition (*e.g.*, NORM and LYM) while [HistoDiffusion without unconditional large-scale pre-training] struggles to synthesize diverse results (*e.g.*, BACK and MUS). Zoom in for better details.